JOURNAL OF MATERIALS SCIENCE 33 (1998) 1243–1251

A TEM study of precipitation and related microstructures in friction-stir-welded 6061 aluminium

L. E. MURR, G. LIU, J. C. McCLURE
Department of Metallurgical and Materials Engineering and Materials Research Institute, The University of Texas at El Paso, El Paso, TX 79968 USA

Residual microstructures, including dynamic recrystallization and grain growth structures and a wide range of precipitation phenomena associated with a friction-stir-weld in a thin 6061-T6 aluminium plate have been systematically investigated utilizing light metallography and transmission electron microscopy. In this rather remarkable process, a hard steel head pin rotating at 400 r.p.m. was advanced into a solid 6061-aluminium plate at a traverse velocity of approximately 2 mm s^{-1} to produce a solid-phase weld in its trailing side. Maximum work-piece temperatures did not exceed 425 °C and there was no melt evidence. Dynamic recrystallization associated with the solid-state plastic flow therefore seems to provide the process mechanism. Weld zone hardnesses averaged roughly 55 Vickers hardness number (VHN) in contrast to the base plate or work-piece hardness of 110 VHN. Precipitation microstructures ranged from continuous to discontinuous coherent zones ($\sim$2 nm thick) coincident with $\{1\,0\,0\}$ planes, semicoherent and non-coherent needles and plates characteristic of Widmanstätten structures coincident with $\{1\,1\,0\}$ planes, and a range of homogeneous precipitate particles often intermixed with these microstructures in the effective heat-affected zone (HAZ′) connecting the friction-stir-weld zone with the unaltered work piece microstructures.

1. Introduction

Friction stir welding is a generic description of a rather remarkable phenomenon in which a rotating, hard (steel) pin can be advanced between two contacting metal plates or into a solid section of a continuous plate to create a "weld" in its wake or trailing side as illustrated schematically in Fig. 1 [1–3]. Unlike conventional, thermal, welds, this weld remains in the solid state, i.e. there is no associated melt. This solid-state stirring occurs by extreme plastic deformation which creates high densities of dislocations which are precursors to dynamic recrystallization that characerizes the actual weld zone [4]. Preliminary studies have shown a varied and somewhat complex range of precipitation microstructures in the transition region extending from the friction-stir weld zone and into the original work piece in 6061-T6 aluminium [4]. In this paper, we present a detailed analysis of precipitation and precipitation-related microstructures in friction-stir-welded 6061 aluminium utilizing conventional transmission electron microscopy (CTEM).

2. Experimental details

In the work to be reported in this paper, a 6061-T6 aluminium alloy plate, nominally 0.6 cm thick, was friction stir welded using the arrangement shown in Fig. 1b, using a hardened, carbon steel head-pin (HP) having a diameter of 0.6 cm and a length of 0.58 cm (slightly shorter than the thickness of the work-piece). A head-pin rotational speed (R in Fig. 1) of 400 r.p.m. was employed together with a translational velocity (T in Fig. 1) of 0.2 cm s^{-1} into the solid work piece. The chuck diameter into which the head-pin was inserted (Fig. 1) was 1.9 cm. To some extent, the chuck defines the upper weld dimensions and characteristics because it is in contact with the work piece, and as a consequence provides additional frictional heating at the top of the work piece.

Cross-sections were cut through the experimental weld zone and were cold-mounted, ground, polished, and etched with Keller's reagent (150 ml water, 3 ml nitric acid, 6 ml hydrochloric acid, 6 ml hydrofluoric acid) at 0 °C for light microscopy. Thin specimens were also sliced from these cross-sections at various locations within and outside the weld zone and at various locations within the transition regions between the weld zone and the work piece (effectively the heat-affected zone or HAZ). These various, thin sections were ground to $\sim$0.2 mm thickness, mechanically dimpled, and 3 mm discs punched at specific locations for transmission electron microscopy (TEM) specimen preparation. A Tenupol-3 dual jet electropolishing unit was used to produce electron-transparent thin sections in these punched discs using a 20% nitric acid solution in methanol at -20 °C. CTEM

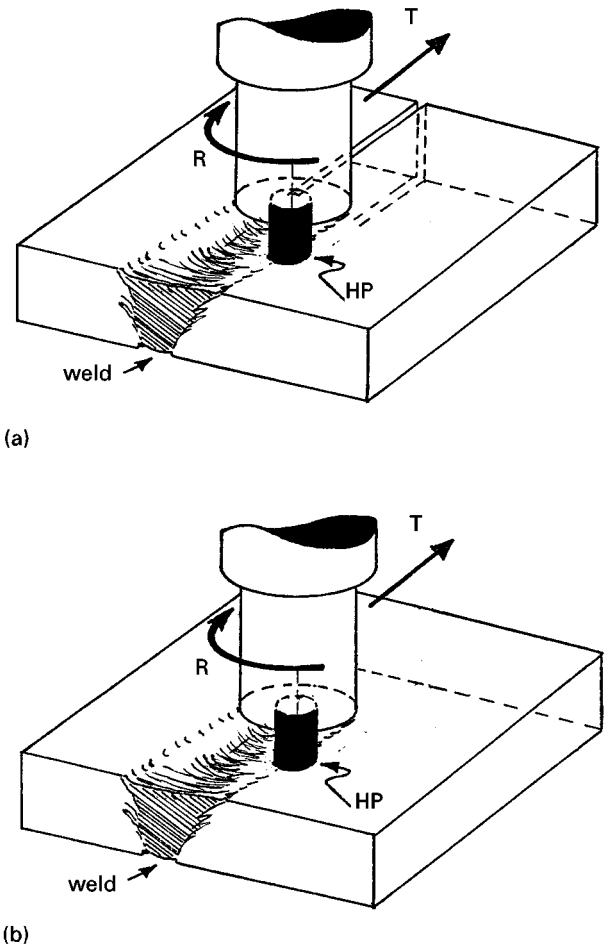

Figure 1 Schematic arrangements illustrating friction stir welding in thin plate. A rotating (R), hard (steel) head-pin (HP) having dimensions essentially equal to the plate thickness advances into the work piece at some selected traverse speed (T) to create a solid-phase weld in its trailing side. (a) Butt weld arrangement. (b) Simple advancement and weld zone development in a solid (continuous) plate section.

was performed in a Hitachi H-8000 instrument operated at 200 kV accelerating potential and employing a goniometer-tilt stage. Energy-dispersive X-ray spectrometry (EDS) was also employed for precipitate analysis in the TEM.

Instrumental (digital) Vickers microhardness measurements were made in Shimadzu hardness testing unit with a 100 gf (0.98 N) load to produce continuous, hardness profiles from the work piece, through the effective heat affected zone (HAZ′), and into the friction-stir-weld zone.

3. Experimental results and discussion

Fig. 2 illustrates a typical section view of a friction-stir weld zone in a 6061 aluminium (continuous) plate section (Fig. 1b). There are some discrepancies or registration irregularities at the base of the weld as a consequence of the slight shortening of the head pin as noted previously, but the weld interior itself exhibits a high degree of continuity and no porosity. The transition region shown in the insert views in Fig. 2b illustrate some aspects of the solid-state plastic flow of work-piece material and the recrystallization which occurs within the weld zone itself as discussed previously [4]. Fig. 3 in fact compares the grain structures and corresponding microstructures within the weld zone centre and the work piece while Fig. 4 compares microhardness traverses through the weld keyed to notations shown in Fig. 2a. The hardness data uniformly illustrates the general softening throughout the dynamically recrystallized weld zone and the hardening associated with the transition or equivalent heat-affected zone (HAZ′). This hardening evolution, which merges with the work-piece or base metal hardness, occurs in large part through precipitation microstructure variations from both the top to the bottom of the "welded" work piece and across or within the transition region (HAZ′) between the weld zone and the work piece. The hardness profiles illustrate a very slight variance within the weld zone centre and from the top to the bottom of the weld. However, the most significant feature of the hardness profiles in Fig. 4 is the apparent width of the transition region influenced by the solid-state flow accommodating the friction stir weld process, which extends well beyond the apparent HAZ illustrated in Fig. 2a. In addition, Fig. 4 illustrates a variation in hardness between the weld zone (and HAZ) and the base or work-piece hardness of roughly 60 VHN ($\Delta H = 110$ VHN $- 50$ VHN) where 1 VHN equals 0.01 GFa. While a comparison of Fig. 3a and d illustrates an average reduction in recrystallized grain size of roughly a factor of 10 (from 100 μm to 10 μm averaging the elongated grains in Fig. 3a and comparing with the equiaxed grains in Fig. 3d) to account for the weld-zone softening in general, the hardness variance shown in Fig. 4 also suggests significant microstructure variations in the regions connecting the base microstructure (Fig. 3b and c) with the weld-zone microstructure (Fig. 3e).

In contrast to a very high dislocation density in the workpiece locations far removed from the weld zone as shown in Fig. 3b and c the dislocation densities in or near the weld zone are considerably reduced as shown for comparison in Fig. 3e from the weld centre, and in Fig. 5 which shows views moving away from the weld centre toward the transition region or apparent HAZ. Figure 5b and d also show variations in the precipitation behaviour and morphology on moving from the weld zone centre. This variation in precipitation becomes even more dramatic in moving into the HAZ as illustrated in Figs 6 and 7. A comparison of Figs 6 and 7 also provides an explanation for the hardness variations from the weld bottom to the top because the magnifications of the images in Figs 6 and 7 are essentially identical, and the density differences are therefore quite apparent (a considerably higher density in Fig. 7 near the top of the plate).

Both Figs 6 and 7 show classical Widmanstätten structures characteristic of semi-coherent and non-coherent precipitation strengthening microstructures. These are characterized by thin, non-coherent needles and plates in Fig. 6 while those in Fig. 7 are essentially all fine, semi-coherent needles (especially notable in Fig. 7a). The crystallographic orientations in Figs 6 and 7 are identical, and the precipitates lie in identical traces of $\{1\,1\,0\}$ planes. Fig. 6c shows a dark-field

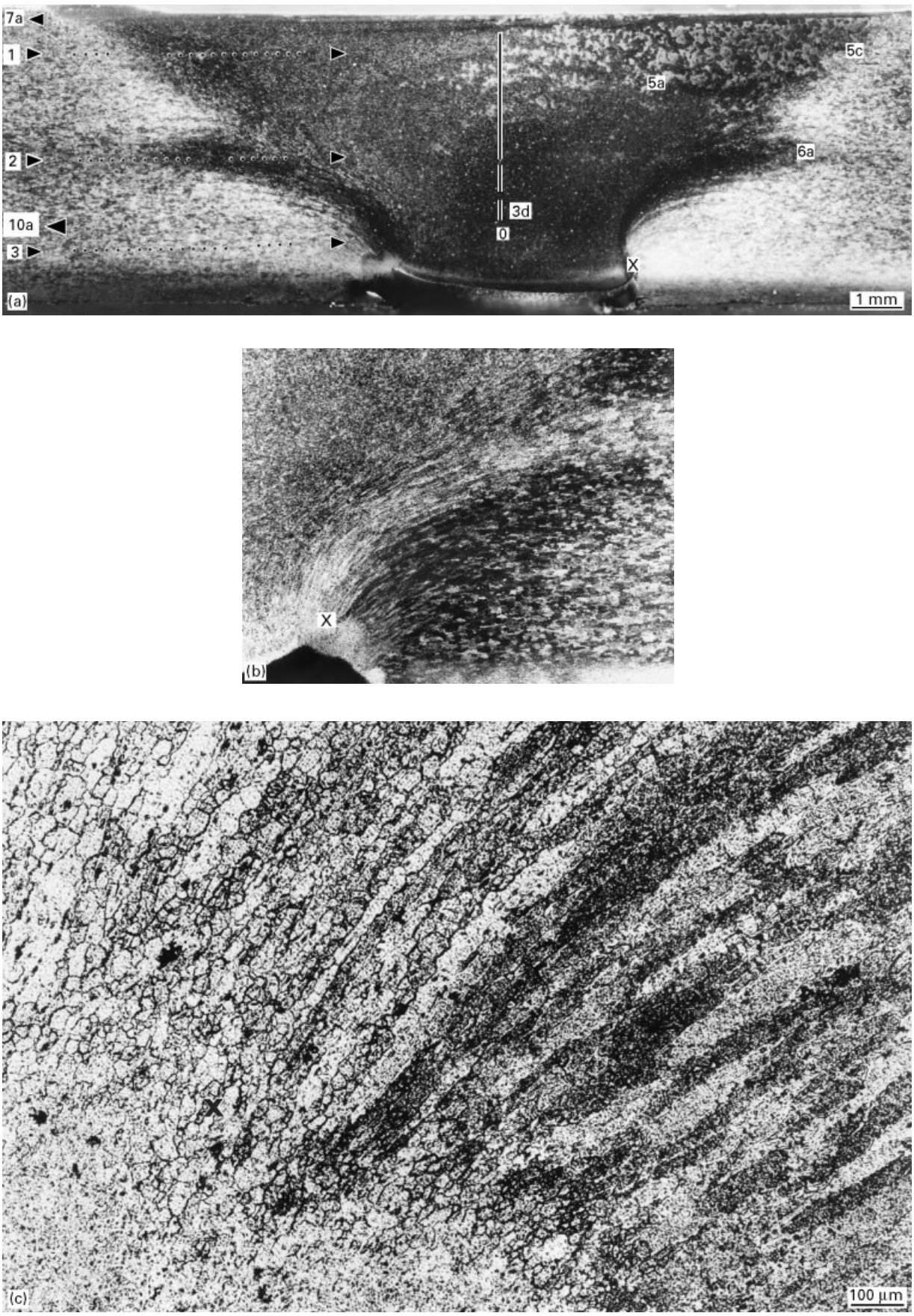

Figure 2 Friction stir-weld zone cross section. (a) Low magnification, thru-thickness view. Locations of horizontal microhardness traverses through the weld zone are shown by arrows and dotted lines with keys marked 1, 2, 3. Locations of microstructure views keyed to figure captions are also noted. (b) Magnified views at x in (a). (c) Shows a magnified view of x in (b).

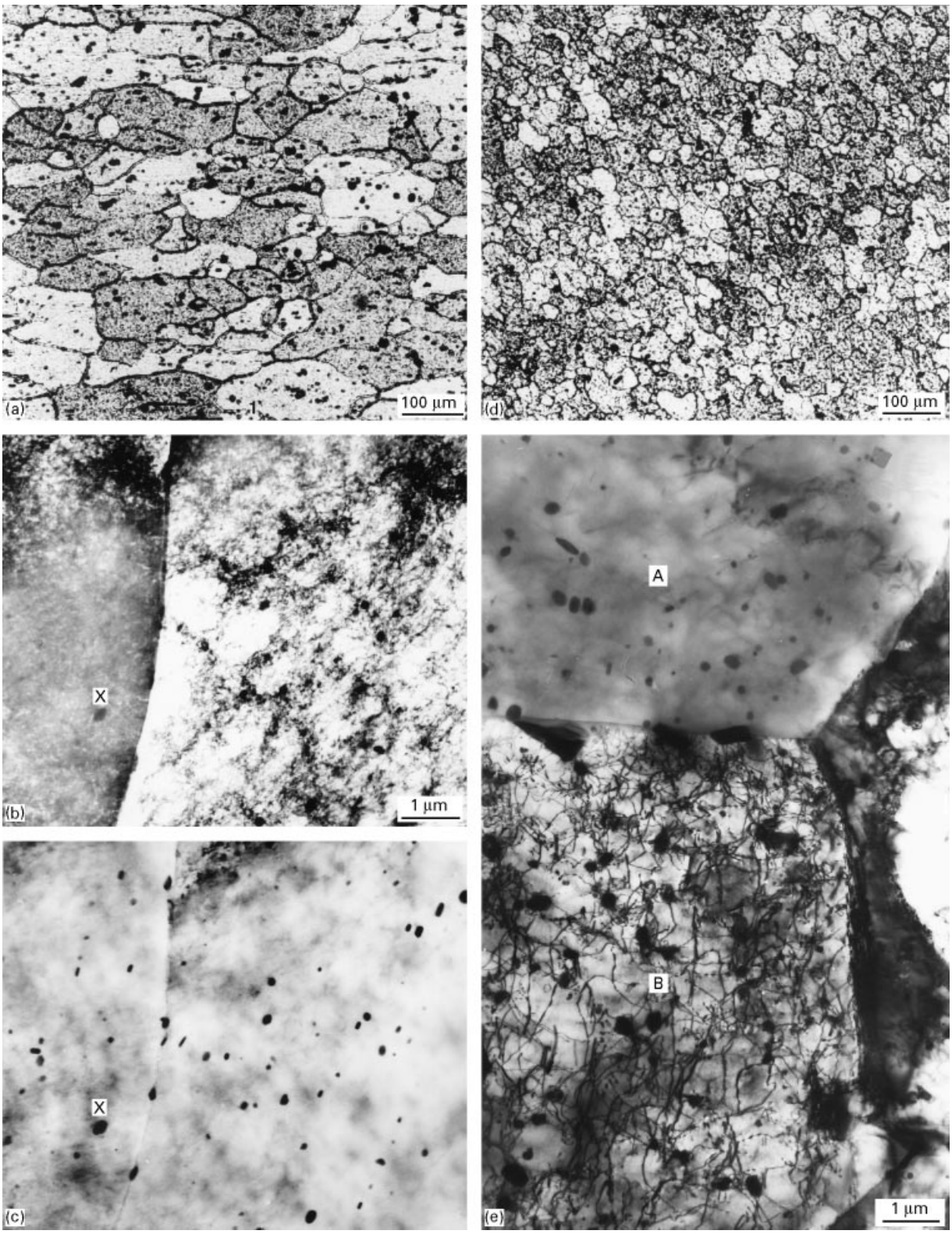

Figure 3 Comparison of light microscope and transmission electron microscope images of friction stir weld zone and base plate (work piece) microstructures. (a) Light microscope view of work piece grain structure. (b) Typical workpiece microstructure in the TEM; far removed from the friction stir weld region. (c) Tilted view (TEM) of (b) where dislocation contrast is essentially zero ($\mathbf{g}.\mathbf{b} = 0$) revealing the precipitates. (d) Light microscope image of equiaxed, recrystallized grain structure in weld-zone centre marked 3d in Fig. 2(a). (e) TEM bright-field image of friction stir weld zone centre as in (d). The upper grain marked A is tilted for no dislocation contrast ($\mathbf{g}.\mathbf{b} = 0$) while the lower grain marked B is strongly diffracting and exhibits strong dislocation contrast.

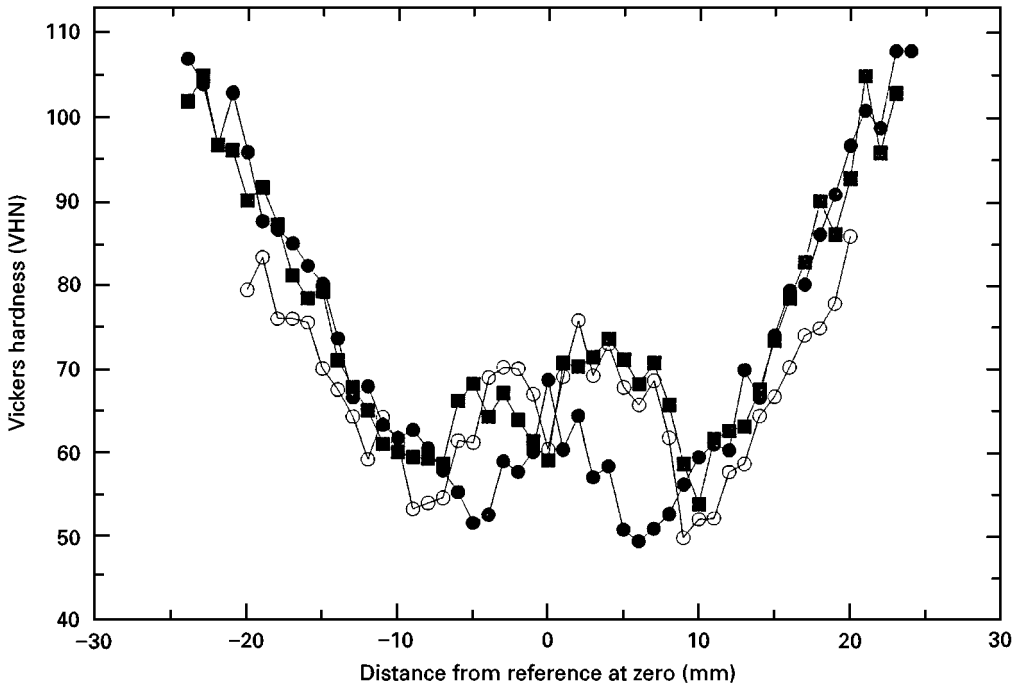

Figure 4 Vickers microhardness profiles extending along horizontal reference lines marked 1 (■), 2 (○) and 3 (●), in Fig. 2a. Note also horizontal reference line through the weld centre marked zero (0) in Fig. 2a.

image recorded by including two separate precipitate reflections shown circled in the selected area diffraction (SAD) pattern insert in Fig. 6b. Fig. 6a is also indicative of a high density of dislocations and very small dislocation loops (as small as 2.0 nm), all characteristic of the dynamic ageing which apparently accompanies the plastic flow and dislocation motion and interaction which facilitates the friction stir weld zone formation.

Figs 8 and 9 illustrate other Widmanstätten structure orientations in contrast to Figs 6 and 7, but in addition illustrate these dynamically aged precipitate needles and thin plates coincident with traces of $\{1\,1\,0\}$ planes associated with the range of equilibrium precipitate particles and some very large precipitates associated with the grain boundaries. While it is not known with any certainty that the grain boundary region shown in Fig. 8 represents a remanent work-piece grain boundary or a recrystallized grain boundary formed in the friction-stir weld process, there is a noticeable depletion or denuding of precipitates in the grain boundary region. Energy-dispersive X-ray spectrometry using a fine-focused electron beam in Fig. 8 and similar regions generally indicate the very large precipitates in or near the grain boundary to be AlSi or MgAlSi. The homogeneously distributed precipitates, including the Widmanstätten precipitates in Fig. 8 (as well as the homogeneous precipitates shown in Fig. 3c and e) are generally $MgAl_xSiCu$; where x seems to vary from around 8 to 10. Some large precipitates have a composition near $Fe_2Al_4MgSiCu$.

Finally, at distances considerably removed from the weld zone centre ($\sim$10 mm) and especially near the weld bottom or in the work-piece bottom, especially thin and primarily coherent needles were observed. These needles have features very similar to classic Guinier-Preston (GP)-type (precipitation) zones or somewhat more developed precipitation zones. These microstructural features are illustrated typically in Fig. 10 which shows needles having average thicknesses of about 2.0 nm and lengths extending to 0.5 μm. Consistent with classical coherent precipitation zones, the needles in Fig. 10 are coincident with the $\{1\,0\,0\}$ planes, as unambiguously demonstrated by the [0 0 1] zone SAD patterns inserted in Fig. 10a, c, and d. Fig. 10c also illustrates the occurrence of complex precipitate shapes intermixed with the coherent, $\{1\,0\,0\}$-oriented needles. Fig. 10b shows an enlarged view of Fig. 10a showing prominent strain-field contrast along the length of the needles corresponding to $\pm\,\mathbf{g} = \langle 2\,0\,0\rangle$ operating reflections. Fig. 10d, by contrast, shows similar, but thicker $\{1\,0\,0\}$ coincident precipitate zones which are essentially non-coherent (with $\mathbf{g} = [2\,0\,0]$ and [0 2 0] from the [1 0 0] zone SAD insert).

Since the precipitate zone volumes in Fig. 10 are so small, it was not possible to determine their compositions either from SAD pattern analysis or EDS analysis. However, it is likely that the compositions differ from the Widmanstätten precipitates shown in Figs 6 to 9.

If we examine the range of precipitates and precipitation morphology and evolution in retrospect, it is apparent that the microstructures associated with a friction stir weld in a thin 6061 aluminium plate cover the entire range of classic precipitation, including continuous, discontinuous, and localized precipitation; and from $\sim$2.0 nm precipitation zones, to needles, thin plates, particulates, and other complex shapes. The evolutionary features and diversity of precipitation is especially apparent on systematically re-examining Figs 3 and 5 to 10 in either a forward or

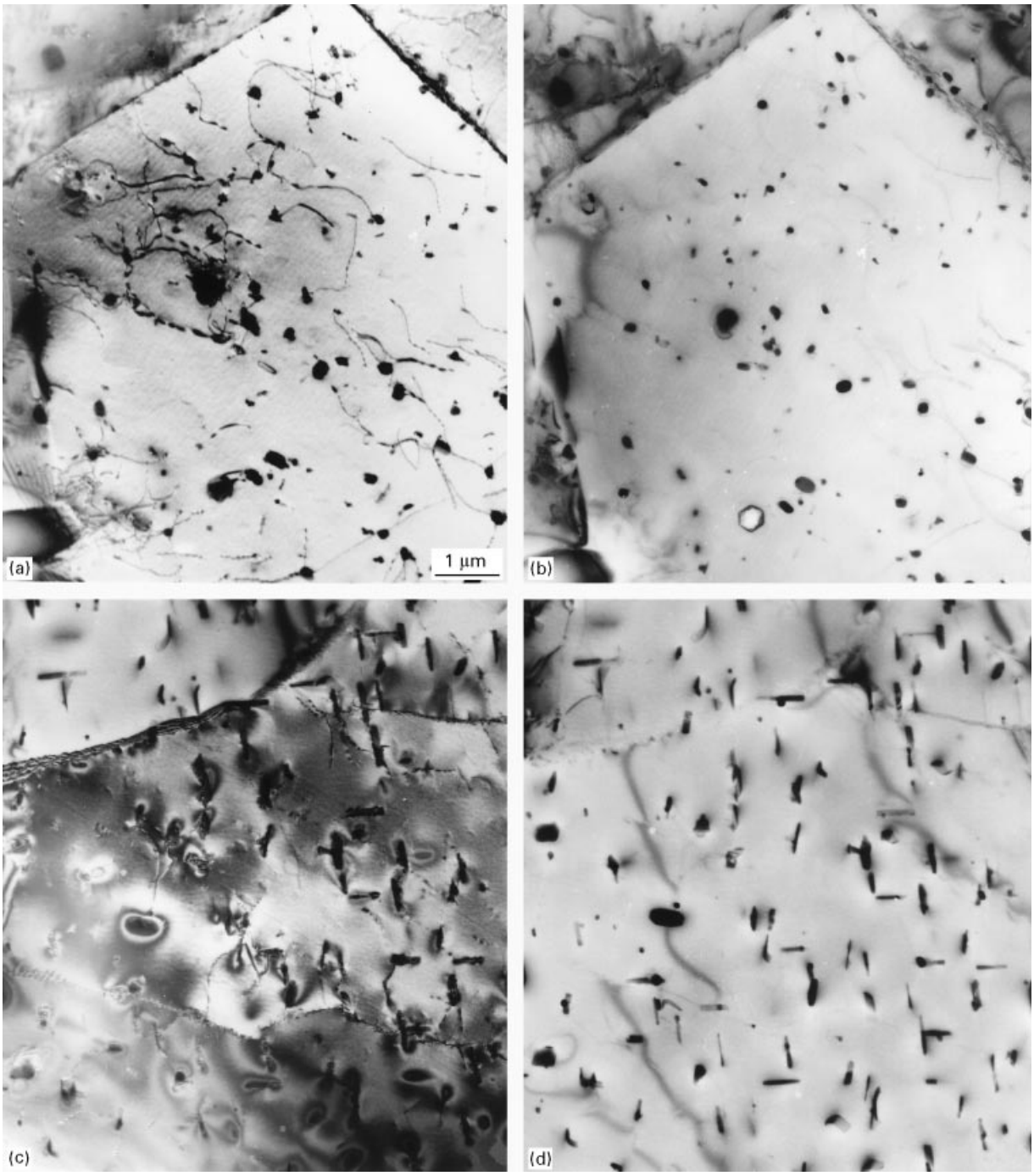

Figure 5 Variation of homogeneous precipitation on moving outward from the weld-zone centre toward the HAZ′. (a) TEM bright-field image at 5a in Fig. 2a. (b) Tilted image of (a) for no dislocation contrast. (c) TEM bright-field image at 5c in Fig. 2a. (d) Tilted image of (d). Note that (c) and (d) are on the transition between the weld zone and the work piece (HAZ′).

reverse order extending from the weld zone to the work piece or vice versa. While Fig. 10 seems to be very closely related to more advanced GP-type (precipitation) zones, the specific nature (and composition) and crystallography of these precipitate zones are unknown. In addition, while maximum temperatures near the top surface and centre of the weld zone have been measured to be around 425 °C, temperature variations within the stir-weld region in the 6061 Al plate are not accurately known and it is difficult to speculate about specific ageing phenomena. Nonetheless, the wide variation in precipitation microstructures shown in Figs 3 and 5 to 10, as well as the corresponding and associated microhardness variations shown in Fig. 4, are an indication of the wide influence of the friction stir weld process on the work piece. That is, the HAZ′ extends well beyond the dimensions of the weld zone; roughly four times the diameter of the headpin (Fig. 1) near the top surface of the work piece plate.

Figs 3 and 5 tend to suggest that while dynamic recrystallization (and grain growth) play a dominant role in the creation of the friction-stir weld zone, there is not much variation in the homogeneity and other features of precipitate particles from the work piece, and these precipitates in fact seem to be stirred into the weld zone from the work piece, although the

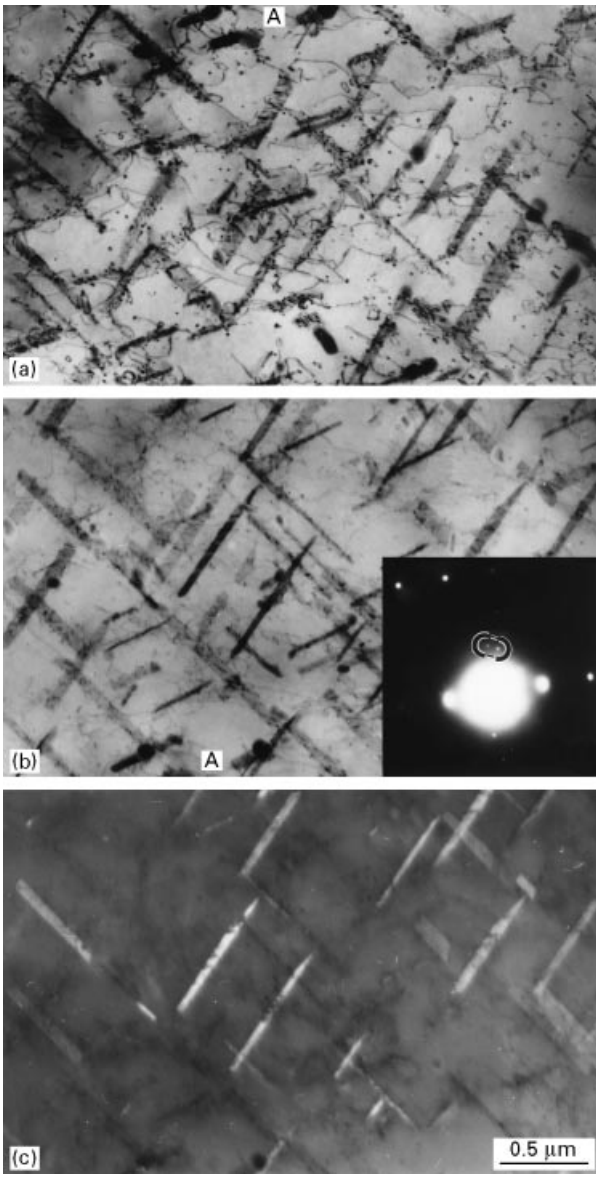

Figure 6 TEM image sequence of precipitates at the edges of the friction-stir weld zone shown at 6a in Fig. 2a. This region is below the precipitates shown in Fig. 5c and d but near the plate centre. (a) Bright-field image showing dislocation and loop contrast along with precipitates shown in Fig. 5c and d but near the plate centre. (a) Bright-field image showing dislocation and loop contrast along with precipitate contrast. Small black dots are very small precipitates (~2.5 to 5.0 nm in diameter). Larger dislocation loops exceed 100 nm in diameter. (b) Tilted view of (a) showing [5 1 1] zone axis SAD pattern insert. (c) Dark-field image of (b) using two precipitate reflections shown circled in the SAD insert in (b). Reference areas in (a) and (b) are shown by A.

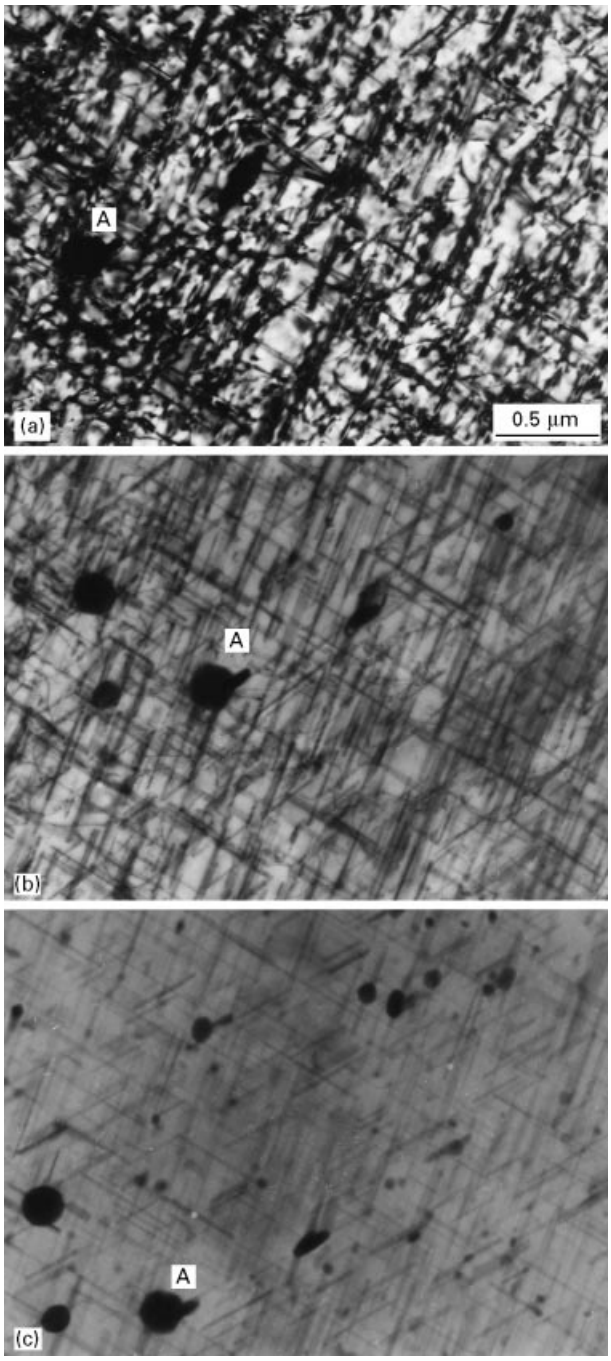

Figure 7 Dense, semi-coherent Widmanstätten-type precipitate structure located at 7a in Fig. 2a near the upper-left work-piece surface, and extending into the base plate. (a) TEM bright-field image crystallographically identical to Fig. 6. (b) Tilted from (a). (c) Tilted from (b). Reference areas are marked A in each image.

degree of exsolution and reprecipitation is unknown. It may be that variations in head pin rotational speed as well as translational velocity will have a noticeable influence on the precipitation features which in turn may influence the weld strength and integrity. It is apparent on comparing Fig. 4 with the range of precipitation microstructures that hardness variations from the weld zone and extending into the work piece are at least in large part related to the precipitation hardening which occurs in this regime, especially by Widmanstätten structures as shown in Figs 7 and 9.

4. Conclusions

The friction-stir welding of 6061-T6 plate is characterized by a range of microstructures including dynamic recrystallization and grain growth (producing an average grain size reduction from the base plate by a factor of 10) within the actual weld zone, as well as a significant reduction in the dislocation density which leads to considerable softening in contrast to the base plate or work piece. In addition to homogeneous precipitates stirred into the weld zone by solid-state flow, there is a wide range of continuous and discontinuous precipitates consisting of 2.0 nm thick coherent

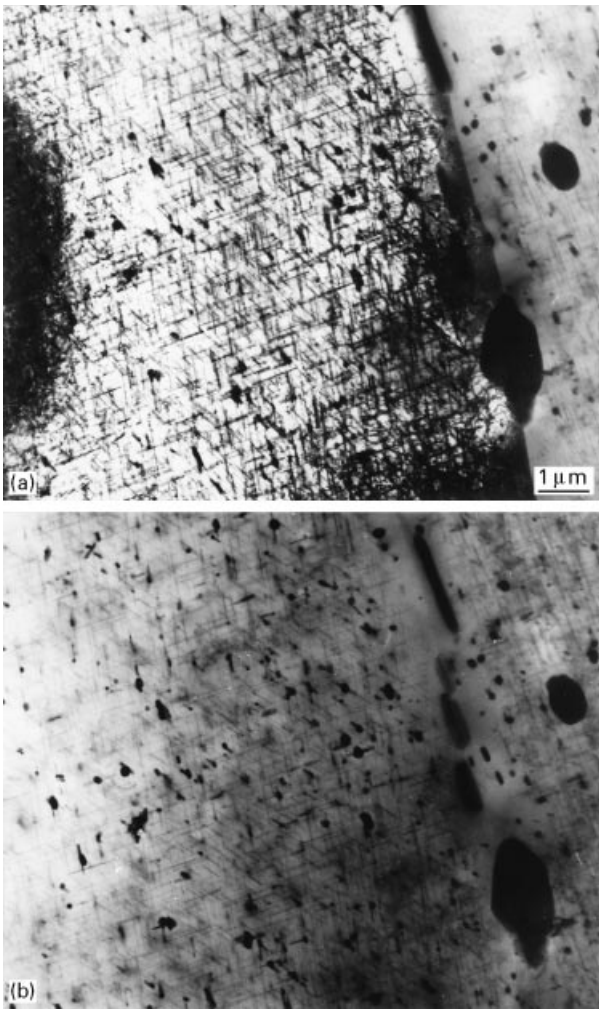

Figure 8 Dense Widmanstätten structure typical of the region marked 8a in Fig. 2a near the bottom of the base plate, and outside the weld zone. (a) TEM bright-field image with a [1 1 2] zone axis. (b) Tilted image in (a) to high-light homogeneous precipitates intermixed with Widmanstätten precipitates and grain boundary precipitates.

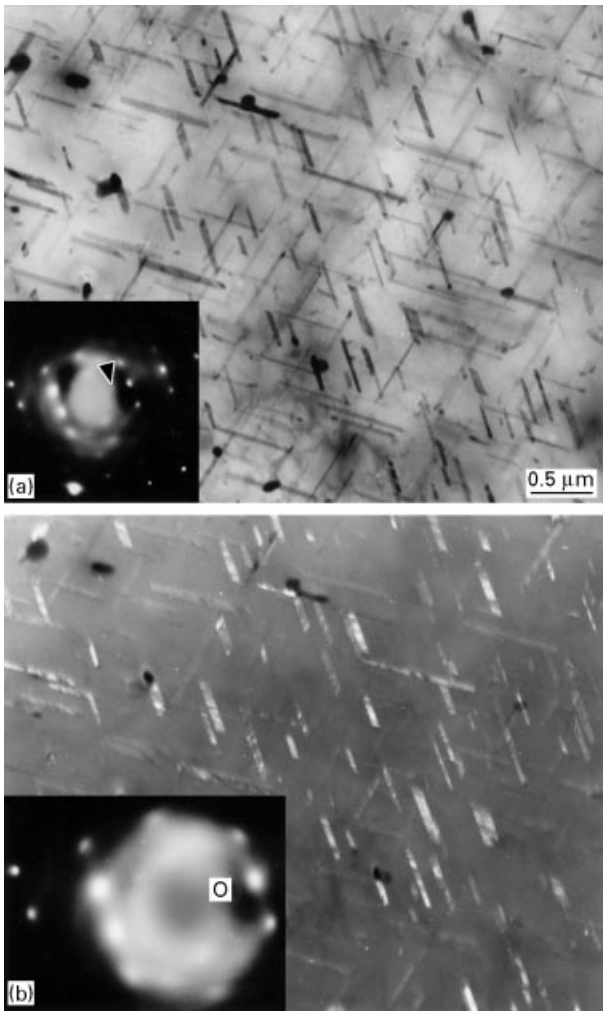

Figure 9 Magnified view of Widmanstätten precipitates in [1 1 2] zone near Fig. 8. (a) TEM bright-field image with SAD pattern insert showing $\pm g = \langle 1\,1\,1 \rangle$. (b) Dark-field image of (a) utilizing precipitate reflection indicated in enlarged SAD pattern insert in (a) (also shown enlarged in (b)).

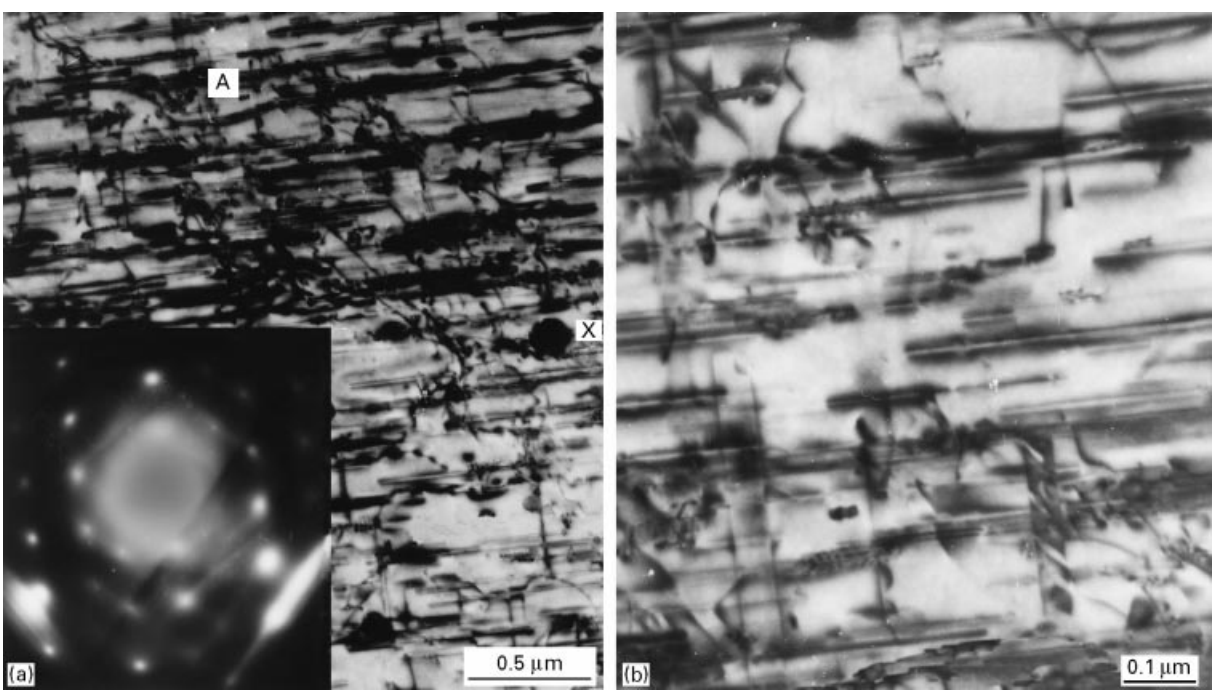

Figure 10 (Continued)

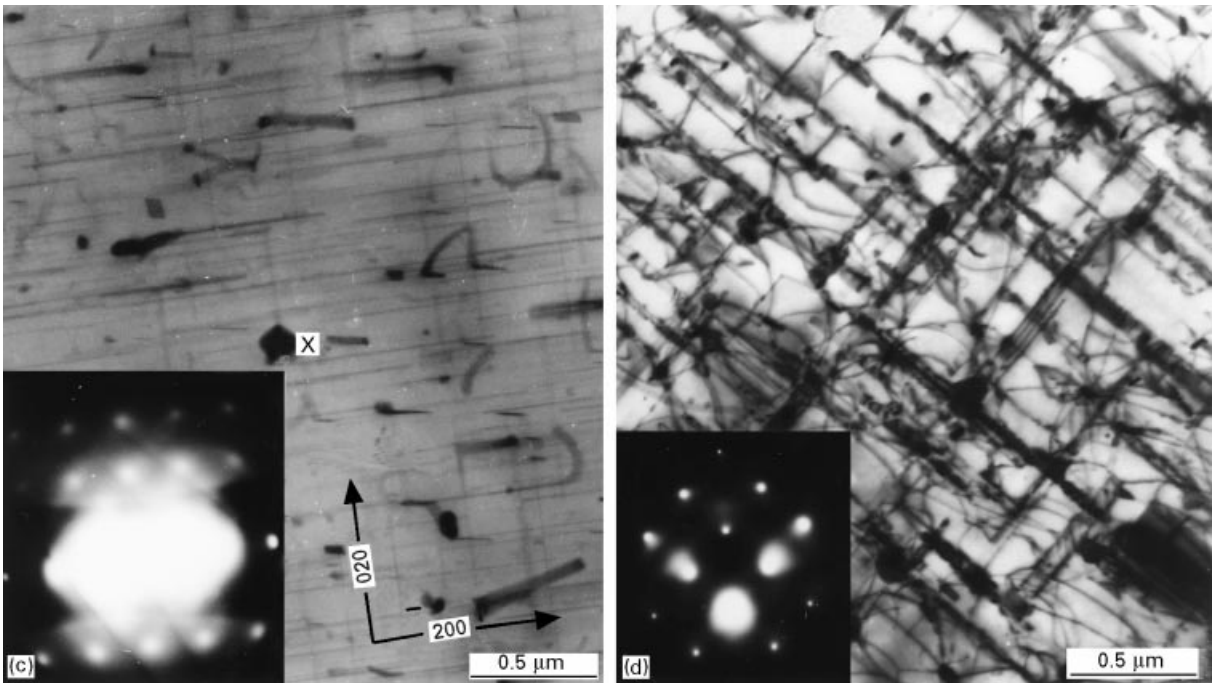

Figure 10 Sequence of bright-field TEM images showing {1 0 0} coincident coherent and non-coherent needle precipitates, located at or near 10a in Fig. 2a. This location is actually farthest from the actual weld zone and possibly in the coolest portion of the work piece plate (near the bottom of the plate. (a) Dense, coherent precipitate coincident with {1 0 0} plane trace directions. SAD pattern insert shows [0 0 1] zone axis. (b) Magnified view of reference region marked A in (a) showing linear strain-field contrast. (c) Tilted image of (a) showing actual precipitate zone widths along both [2 0 0] and [0 2 0] directions. Reference areas are denoted × in (a) and (c). (d) Similar but non-coherent precipitate zones coincident with {1 0 0} planes. SAD pattern insert illustrates the [0 0 1] zone axis.

and crystallographically coincident precipitate zones, thin, semi-coherent and non-coherent needles and plates coincident with {1 1 0} matrix planes, as well as other, complex precipitate shapes intermixed with both homogeneous precipitates and Widmanstätten structures involving crystallographically coincident precipitate needles and thin plates. These precipitation structures and crystallographic distributions provide a variation in residual microhardness extending from the friction-stir weld zone and into the work piece. There is no evidence for melt in this rather unique, solid-state plastic flow phenomena, where maximum temperatures near the work piece and weld-zone top surface have been measured to be around 425 °C.

Acknowledgements

This research was supported in part by a NASA-Marshal Space Flight Center Grants NAG-8-1056 and NCC-8-137; and by a Mr and Mrs MacIntosh Murchison Chair Endowment (L.E.M.) at The University of Texas at El Paso. We are grateful for the assistance of Dr C.-S. Niou and Mr F. R. Vega during the early stages of developing the experimental welding arrangements and procedures.

References

1. W. M. THOMAS, E. D. NICHOLAS, J. C. NEED HAM, M. G. MURCH, P. TEMPLESMITH and C. J. DAWES, International Patent Application No. PCT/GB92/02203 and GB Patent Application No. 9125978.8, Dec. 6, 1991.
2. O. T. MIDLING, in Proceedings of the 4th International Conference on Aluminium Alloys (ICAA4), Atlanta, GA, USA, 11–16, September, 1994.
3. C. J. DAWS, *Welding & Metal Fabrication* **January** (1995) 12.
4. G. LIU, L. E. MURR, C.-S. NIOU, J. C. MCCLURE and F. R. VEGA, *Scripta Mater.*, **37** (1997) 355.

Received 26 March
and accepted 24 September 1997